Eur. Phys. J. B **44**, 259–264 (2005)
DOI: 10.1140/epjb/e2005-00122-7

THE EUROPEAN PHYSICAL JOURNAL B

Transition from coherent rotation to curling mode reversal process in ferromagnetic nanowires

S. Goolaup[1], N. Singh[1,2], A.O. Adeyeye[1,a], V. Ng[1], and M.B.A. Jalil[1]

[1] Information Storage Materials Laboratory, Department of Electrical and Computer Engineering, National University of Singapore, 4 Engineering Drive 3, Singapore 117576
[2] Institute of Microelectronics, 11 Science Park Road, Singapore Science Park II, Singapore 117685

Received 2 November 2004 / Received in final form 24 January 2005
Published online 20 April 2005 –

Abstract. We have investigated the evolution in the magnetization reversal mechanism of lithographically defined $Ni_{80}Fe_{20}$ nanowire arrays with varied film thicknesses. The nanowire array of width 185 nm and spacing 35 nm were fabricated using deep ultraviolet lithography at 248 nm exposing wavelength. We observed a cross-over from coherent rotation to curling reversal mode when the thickness to width ratio $\geq$ 0.5. We have aided our understanding of the reversal process with theoretical modeling. A marked increase in the coercive field characterized the intermediate region between coherent rotation and magnetization curling.

PACS. 75.30.Gw Magnetic anisotropy – 75.60.Jk Magnetization reversal mechanisms – 75.75.+a Magnetic properties of nanostructures

1 Introduction

Recently, there has been considerable interest in the fabrication and study of magnetic nanostructures due to their unique properties as compared to bulk materials. One class of nanomagnets that has been gaining a lot of attention is nanowires. There is growing interest in magnetic nanowire both from a fundamental viewpoint and because of their potential applications in magnetoelectronic devices.

There are various techniques for fabricating magnetic nanowires. These include electron-beam lithography and lift-off technique [1,2], epitaxial growth on single crystal [4] and electrodeposition on nanoporous template [4–13]. The main problem with electron-beam lithography is that it is very difficult to fabricate closely packed high aspect ratio nanowire arrays due to proximity effects. Moreover, the writing process in electron beam lithography is serial and very slow, thus making large area fabrication very difficult. Electrodeposition offers a cheap and simple way to fabricate arrays of cylindrical nanowires. The main limitation of electrodeposition technique is the distribution of pore size and orientation of the nanoporous membranes [9]. This makes the orientation and spacing of the nanowires difficult to control. Thus, quantitative information about the magnetic properties and the exact magnetization reversal process can not be readily obtained.

In this paper, we present the magnetic properties of closely packed nanowire arrays fabricated using deep ultra violet (DUV) lithography and lift-off process. The advantage of this fabrication technique is that it is a parallel process and highly ordered nanowire arrays can be fabricated over a very large area as compared to currently available techniques. This makes characterization of magnetic properties using various magnetometry techniques possible. We have used this technique to fabricate 10–180 nm thick $Ni_{80}Fe_{20}$ nanowire arrays of width $w = 185$ nm and inter-wire spacing $s = 35$ nm over an area of 4×4 mm^2. Scanning Electron Microscope (SEM) was used to verify the lateral dimensions of the wires. The magnetic properties of the nanowire arrays were measured using Vibrating Sample Magnetometer (VSM). We have investigated the thickness dependence of the magnetization reversal process by keeping the wire dimensions fixed and varying the thickness of $Ni_{80}Fe_{20}$ films deposited. We observed that the demagnetizing field due to shape anisotropy dominates the magnetization reversal process in $Ni_{80}Fe_{20}$ nanowire arrays. Based on the field orientation dependence of the coercivity, a cross over from coherent rotation mode dominated reversal to curling mode of magnetization reversal was observed when thickness to width, t/w, ratio ≥ 0.5.

2 Experimental method

In our experiments, the $Ni_{80}Fe_{20}$ nanowires were fabricated on commercially available Si substrate. To create

[a] e-mail: eleaao@nus.edu.sg

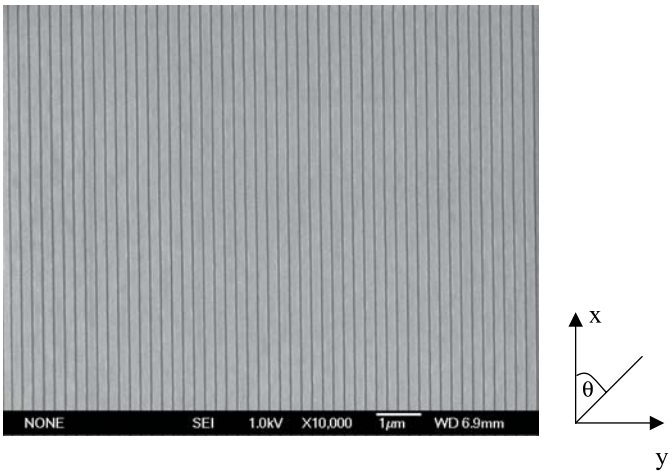

Fig. 1. SEM Micrograph showing the lateral dimensions of the nanowire arrays.

patterns in resist, the substrate was coated with 60 nm thick anti-reflective layer followed by a 480 nm positive DUV photoresist. Nikon lithographic scanner with KrF excimer laser radiation was used for exposing the resist. The wire pitch on the mask was kept at 220 nm. A high-purity alloy source of the nominal $Ni_{80}Fe_{20}$ composition was used to grow permalloy film on the patterned sample by electron beam deposition method. The film was deposited at a rate of 0.4 Å/s and the pressure during growth was maintained at 2×10^{-6} torr. Lift-off of the deposited film was carried out in OK73 solution placed in an ultrasonic bath. Completion of the lift-off process was determined by the color contrast of the patterned $Ni_{80}Fe_{20}$ area and confirmed by inspection under SEM. Details of the fabrication process are described in reference [14].

Figure 1 shows the SEM image of the magnetic nanostructure. The wires are of width 185 nm with inter-wire spacing of 35 nm. The nanowire arrays have uniform width and inter-wire spacing as can be clearly observed from the SEM micrograph. The magnetic characterization using VSM was carried out at room temperature with a maximum applied field of ±5 kOe. Angular dependent measurements were also performed by varying the orientation of the applied field relative to the nanowire easy axis from 0° to 360° in steps of 15°.

3 Results and discussions

3.1 Shape anisotropy

In order to investigate the effect of shape anisotropy, magnetization loops of the nanowire arrays with magnetic field applied parallel and perpendicular to the wire axis were measured. Figure 2a shows the normalized M-H loops for 100 nm thick $Ni_{80}Fe_{20}$ nanowire arrays for field orientation at $\theta = 0°$ and $\theta = 90°$. The corresponding M-H loops of a reference unpatterned sample that was deposited under the same conditions as the nanowire arrays are shown

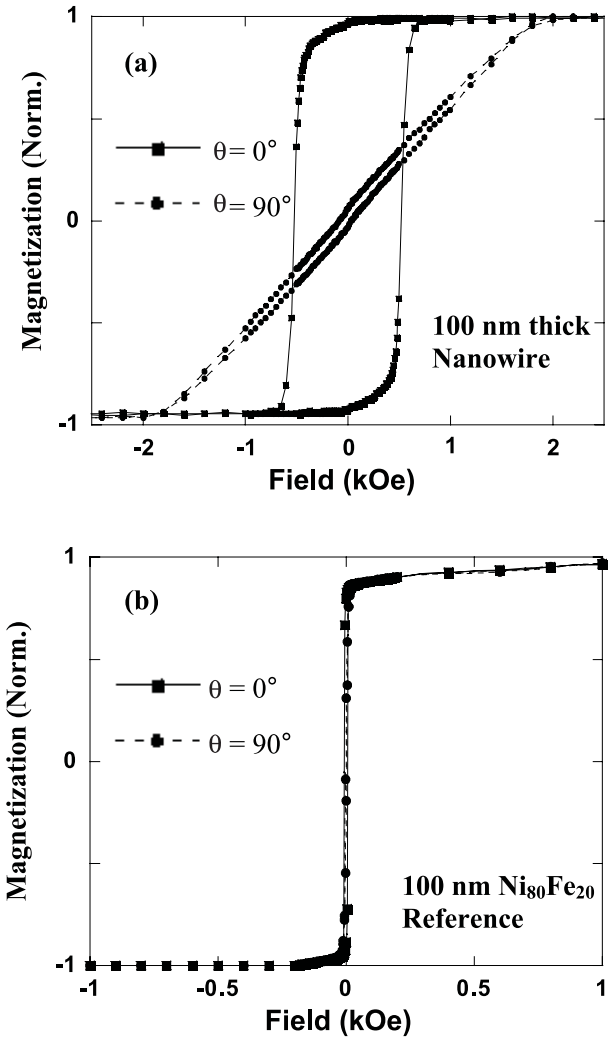

Fig. 2. M-H loops with field applied along $\theta = 0°$ and $\theta = 90°$ for 100 nm thick $Ni_{80}Fe_{20}$ film (a) as nanowire array and (b) as reference sample.

in Figure 2b. We observed that the M-H loops of the reference film are almost the same for both field orientations and displays negligible coercive field as expected. This implies that the reference sample has negligible intrinsic anisotropy as compared with the shape anisotropy of the nanowire.

When the applied field is along the wire axis ($\theta = 0°$), the nanowire array exhibits a rectangular hysteresis loop with a high squareness ratio of 0.97 and an enhanced coercive field of 520 Oe which is much larger than for bulk material. For field applied perpendicular to the wire axis ($\theta = 90°$), a sheared M-H loop with a very small coercive field, 55 Oe and squareness ratio, 0.04 is obtained. A marked increase in the saturation field of the M-H loop is obtained in comparison with the loops obtained for field applied along the wire axis and the reference film. This is attributed to the shape anisotropy being the dominant anisotropy for the nanowire arrays, with the easy axis along the wire axis.

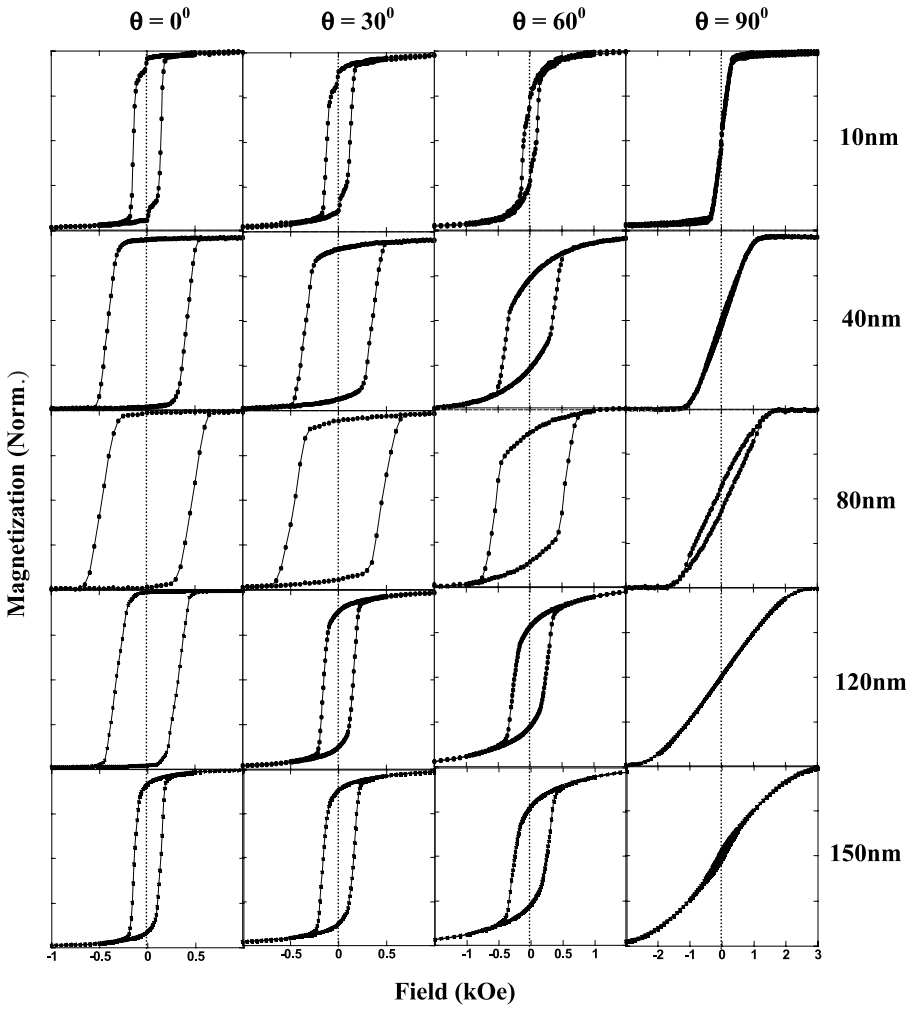

Fig. 3. Representative M-H loops of nanowire arrays of different thickness as a function of the orientation of applied field.

3.2 Thickness-dependent magnetization reversal

We investigated the effect of nanowire film thickness on the magnetization reversal, by varying the thickness of the film while keeping the wire width and inter-wire spacing fixed. We carried out systematic angular measurement of the magnetic properties of the nanowires for thickness ranging from 10 nm to 180 nm. Shown in Figure 3 are the representative hysteresis loops of nanowire as a function of film thickness (t) and also the field orientation (θ). When the field is applied along the nanowire easy axis, $\theta = 0°$, we observed that the coercivity is strongly dependent on the thickness of the film. In the film thickness range 10 nm $\leq t \leq$ 80 nm, there is an increase in the coercivity as the thickness is increased. However, for $t \geq 80$ nm, the coercivity begins to decrease as thickness is increased.

In order to further understand the trend in the coercivity as a function of thickness, we have extracted the coercivity from the M-H loops for $\theta = 0°$ as a function of thickness. Shown in Figure 4, is the plot of coercivity as a function of thickness to width (t/w) ratio for $\theta = 0°$. The coercive field increases with t/w ratio first but decreases after reaching a peak. The peak coercivity and corresponding t/w ratio are respectively 520 Oe and 0.54. This non-monotonic thickness to width ratio, t/w, dependence suggests that there may be a cross-over in magnetization switching mode as the thickness of the film is increased.

For field applied along the hard axis $\theta = 90°$, we observed an evolution in the hysteresis loops as the film thickness is increased. The shape of the M-H loop changes from sharp switching for $t = 10$ nm to a highly sheared loop as the film thickness is increased to $t \geq 40$ nm. The hysteresis loop becomes more S shaped, leading to an increase in saturation field for $t \geq 80$ nm. This can be explained by the strong influence of the demagnetizing field across the wire width. The hard axis saturation field, H_s is given by [15]:

$$H_s \approx H_k + \frac{3}{2} H_d \tag{1}$$

where H_k is the magnetic anisotropy constant, which is negligible in our structures and H_d represents the average demagnetizing field. For wire arrays, the demagnetizing

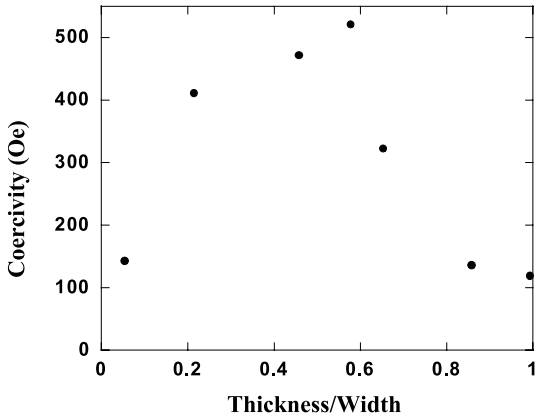

Fig. 4. Coercivity of the nanowire as a function of thickness/width ratio.

field is given by [16]:

$$H_d = 4\pi Ms\frac{t}{w}\alpha(r) \tag{2}$$

where $\alpha(r)$is a function of the ratio of inter-wire spacing to the wire width (s/w). In the limit of $(s/w) \to 0$, the factor $\alpha(r) \to 0$; in the opposite limit of $(s/w) \to \infty$, $\alpha(r) \to 1$. The first limit corresponds to a continuous film, where the wires are in physical contact and the second limit corresponds to isolated wires. For our wire arrays, $s = 35$ nm and $w = 185$ nm; $\alpha(r) \approx 0.34$, a constant value. Thus, the demagnetizing field varies as t/w. As the thickness of the nanowire increases, the demagnetizing field across the wire increases leading to an increase in the saturation field, consistent with our experimental results in Figure 3.

The calculated saturation field, H_s, from equation (1), is slightly larger than the measured field. We attribute this difference to the dipolar interaction among the wires. For moments aligned perpendicular to the wire axis, the total field acting on one wire is the sum of the dipole field and the demagnetizing field of the wire [17]:

$$H_{90} = Hd - 2.1\frac{\mu o}{4\pi}\frac{MsV}{s^3} \tag{3}$$

where V is the volume of the wire. The dipolar interaction causes a smaller effective field along the hard-axis, which may explain the difference in the measured and computed values for saturation field.

3.3 Magnetization reversal modes in nanowire

The angular dependence of coercivity provides information on the magnetization reversal mode. To better understand the evolution of the magnetization reversal modes, we extracted the values of coercive field from the hysteresis loops as a function of the orientation of the applied field for different thicknesses. Shown in Figure 5 is the variation of the coercivity (H_c) with the applied field orientation (θ) for various film thicknesses. Generally, for all

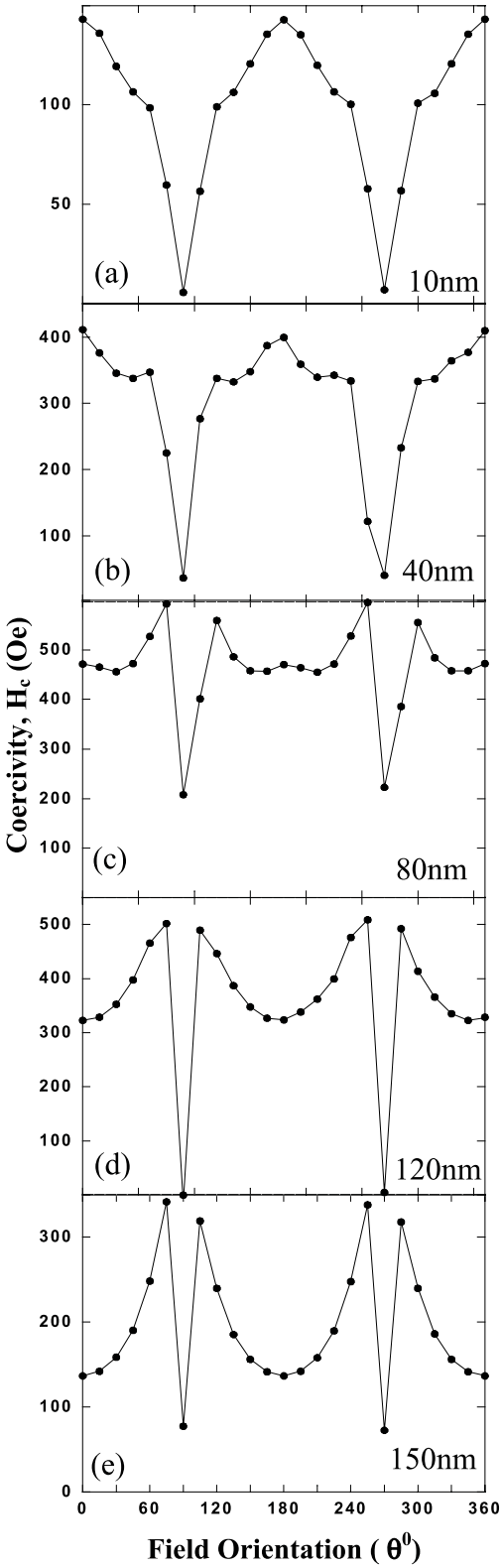

Fig. 5. Coercivity as a function of the field orientation with respect to the wire axis, for thickness ranging from 10 nm to 150 nm.

the thickness range investigated we observed that the coercivity is markedly sensitive to the orientation of the field applied and is symmetrical about field orientation of 180°.

Several mechanisms may be responsible for magnetization reversal: coherent rotation, magnetization curling, magnetization buckling or domain wall motion. For nanowires, two modes are considered as being important; coherent rotation [18] and curling magnetization [19–21]. It is well known that $Ni_{80}Fe_{20}$ is a soft magnetic material with low intrinsic magnetic anisotropy. Since all the wire dimensions are larger than the exchange length [22], we can expect deviations from uniform magnetization and as a result the occurrence of domain wall nucleation at lower fields than the curling field or anisotropy field for field applied along the hard-axis.

For $t = 10$ nm, maximum coercivity occurs for field applied along the nanowire axis ($\theta = 0°$) as shown in Figure 5a. As the field orientation (θ) increases the coercivity decreases, reaching a minimum for field applied along the hard-axis ($\theta = 90°$). This angular variation of coercivity is consistent with the coherent rotation reversal mode based on the Stoner-Wolhfarth model [18]. A bell-shape angular variation is observed as field orientation is varied from $\theta = 90°$ to $\theta = 270°$. As the film thickness is increased to 40 nm, a slight departure from coherent rotation is observed for field orientation of 60° and 120° as shown in Figure 5b. We attribute this departure from coherent rotation as being due to the onset of curling mode of reversal.

Shown in Figure 5c is the H_c vs. θ curve for nanowire array with $t = 80$ nm. A completely different field orientation of the H_c is observed when compared with the coherent mode for $t = 10$ nm. As the field orientation increases from $\theta = 0°$ to $\theta = 30°$, a slight decrease in coercivity is first observed. With further increase in field orientation, an increase in coercivity with a peak at $\theta = 75°$ is observed. For $\theta \geq 75°$ the coercivity decreases to reach a minimum along the hard-axis ($\theta = 90°$). This field orientation dependence of the coercivity may be explained by a combination of coherent rotation and curling mode of magnetization reversal process. The region where there is increase in coercivity with field orientation (i.e $30° \leq \theta \leq 75°$) may be attributed to curling mode reversal [19–21]. The coherent rotation is present for field applied close to the easy and hard axis.

For $t \geq 120$ nm, the coercivity increases as the field orientation increases with respect to the wire axis, reaching a peak for field orientation, $\theta = 75°$ as shown in Figures 5d and e. Beyond this field orientation (i.e. $\theta > 75°$), the coercivity decreases with increasing field orientation, reaching a minimum at $\theta = 90°$. The angular dependence of coercivity could be attributed to curling mode of magnetization reversal process. This is in agreement with result obtained by Han et al. [4].

To aid our understanding of the reversal process of nanowire array with, $t \geq 120$ nm, we modeled our experimental result with the theoretical model proposed in reference [18]. For an infinite cylinder with curling mode of reversal, the coercive field is given as [19]

$$H_c = \frac{M_s}{2} \frac{a(1+a)}{\sqrt{a^2 + (1+2a)\cos^2\theta}} \tag{4}$$

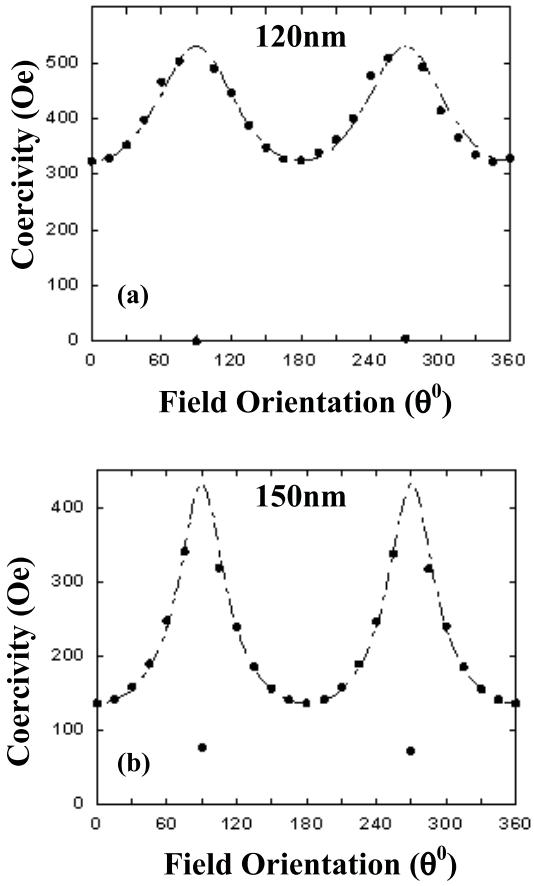

Fig. 6. Angular variation of coercivity together with theoretical prediction, based on curling magnetization, for (a) 120 nm and (b) 150 nm.

where $a = -1.08(d_0/d)^2$. The exchange length $d_0 = 2\sqrt{A}/M_s$. A is the exchange constant. This model is valid for cylindrical wires; however, our structures have rectangular geometry, which is not analytically solvable. We fitted our experimental results with this theoretical model. Shown in Figure 6 is a plot of the experimental data and the theoretical prediction; the dotted line is the predicted coercivity curve for curling mode of magnetization reversal and the dots are the experimental points. There is a very good agreement between the measured coercivity and the theoretical prediction except for field orientation $\theta = 90°$ and $\theta = 270°$. For field applied along the hard axis, a minimum is obtained as opposed to the theoretical prediction of maximum coercive field. This is consistent with the results reported by Han et al. [4], where curling magnetization is present for small θ angles and the coherent rotation occurs at larger θ values. Thus, for thick films, $t \geq 120$ nm, the magnetization reversal is dominated by the curling mode except at large θ, where coherent rotation is responsible for reversal.

In general, we observed that the thickness of the nanowire strongly influences the magnetization reversal mode. As the thickness is increased from 10 nm to 150 nm, there is a gradual change in the magnetization reversal mode from coherent rotation mode at small film

thicknesses to curling mode of magnetization reversal for thicker film. A cross-over from coherent rotation to curling dominated reversal is observed for $t/w \geq 0.5$.

4 Conclusions

We have investigated the reversal processes in ferromagnetic nanowires. Our systematic studies of the effect of the nanowire thickness show that the magnetization reversal mechanism is strongly influenced by thickness of the nanowires. We observed a cross-over from coherent dominated reversal mode to curling magnetization when the thickness to width ratio exceeds 0.5. Moreover, our experimental result agrees well with theoretical modeling of magnetization reversal.

S.G would like to thank the National University of Singapore (NUS) for his research scholarship. The authors would like to acknowledge the support of Dr. Balasubramanian Narayanan of the Institute of Microelectronics, Singapore. This work was supported by NUS Grant No. 263-000-216-112.

References

1. W. Casey Uhlig, Jing Shi, Appl. Phys. Lett. **84**, 759 (2004)
2. A.O. Adeyeye, J.A.C. Bland, C. Daboo, D.G. Hasko, H. Ahmed, J. Appl. Phys. **82**, 469 (1997)
3. H.J. Elmers, J. Hauschild, U. Gradmann, J. Magn. Magn. Mater. **177-181**, 827 (1998)
4. G.C. Han, B.Y. Zong, P. Luo, Y.H. Wu, J. Appl. Phys. **93**, 9202 (2003)
5. I. Chlebny, B. Doudin, J.Ph. Ansermet, Nanostruct. Mater. **2**, 637 (1993)
6. A. Kazadi Mukenga Bantu, J. Rivas, G. Zaragoza, M.A. Lopez-Quintela, M.C. Blanco, J. Appl. Phys. **89**, 3393 (2001)
7. L. Sun, P.C. Searson, C.L. Chien, Phys. Rev. B **61**, 6463 (2000)
8. H. Zeng, M. Zheng, R. Skomski, D.J. Sellmyer, Y. Liu, L. Menon, S. Bandyopadhyay, J. Appl. Phys. **87**, 4718 (2000)
9. J. Meier, B. Doudin, J.Ph. Ansermet, J. Appl. Phys. **79**, 6010 (1996)
10. J. Rivas, A. Kazadi Mukenga Bantu, G. Zaragoza, M.C. Blanco, M.A. Lopez-Quintela, J. Magn. Magn. Mater. **249**, 220 (2002)
11. Wei Chen, Shaolong Tang, Mu Lu, Youwei Du, J. Phys.: Condens. Matter **15**, 4623 (2003)
12. Zhu Hao, Yang Shaoguang, Ni Gang, Yu Dongliang, Du Youwei, J. Magn. Magn. Mater. **234**, 454 (2001)
13. J.M. Garcia, A. Asenjo, J. Velazquez, D. Garcia, M. Vazquez, P. Aranda, E. Ruiz-Hitzky, J. Appl. Phys. **85**, 5480 (1999)
14. N. Singh, S. Goolaup, A.O. Adeyeye Nanotechonolgy **15**, 1539 (2004)
15. C.H. Bajorek, C. Coker, L.T. Romankiv, D.A. Thompson, IBM J. Res. Develop. **18**, 541 (1974)
16. B.B. Pant, J. Appl. Phys. **79**, 6123 (1996)
17. G.J. Strijkers, J.H.J. Dalderop, M.A. Abroeksteeg, H.J.M. Swagten, W.J.M de Jonge, J. Appl. Phys. **86**, 5141 (1999)
18. E.C. Stoner, E.P. Wohlfarth, Philos. Trans. R. Soc. London **240**, 599 (1948)
19. W.F. Brown, Phys. Rev. **105**, 1479 (1957); H. Frei, S. Shtrikman, D. Treves, Phys. Rev. **106**, 446 (1957); S. Shtrikman, D. Treves, J. Phys. France **20**, 286 (1959)
20. A. Aharoni, S. Shtrikman, Phys. Rev. **109**, 1522 (1958)
21. Y. Ishii, J. Appl. Phys. **70**, 3765 (1991)
22. J.K. Ha, R. Hertel, J. Kirschner, Phys. Rev. B. **67**, 224432 (2003)